

# Analysis of Power-to-gas-to-X systems with metal hydride storage based on coupled electrochemical and thermodynamic simulation

Michael Bareev-Rudy<sup>a,\*</sup>, Simon Meiswinkel<sup>a</sup>, Malte Pfennig<sup>a</sup>, Steffen Schedler<sup>a</sup>,  
Barbara Schiffer<sup>a</sup>, Gerd Steinebach<sup>a</sup>, Tanja Clees<sup>a,b</sup>

<sup>a</sup> Hochschule Bonn-Rhein-Sieg University of Applied Sciences, Department of Engineering and Communication, Institute for Technology, Resource and Energy-efficient Engineering (TREE), Grantham-Allee 20, 53757, Sankt Augustin, Germany

<sup>b</sup> Fraunhofer Institute for Algorithms and Scientific Computing SCAI, Schloss Birlinghoven, 53757, Sankt Augustin, Germany

## ARTICLE INFO

### Keywords:

Power-to-gas-to-X  
HESS  
Metal hydride storage  
PEM  
Parameter calibration  
Energy network simulation  
DAE solver

## ABSTRACT

Power-to-gas-to-X systems consisting of photovoltaic cells, proton-exchange membrane electrolysis, hydrogen storage based on metal hydrides, proton-exchange membrane fuel cells and buffer batteries could be used to meet heat and electricity demands of homes, businesses, or small districts. The actual size of the individual components and their interplay have to be optimized for the technical and economic feasibility of the overall system. A simulation-based optimization workflow would be a suitable way to accomplish this task, but there are hardly any tools that can simultaneously simulate power, fluid and heat flows of such systems and efficiently perform their optimization. In this paper, a multiphysical energy system simulation and optimization tool is introduced which models electrochemical and thermodynamic processes simultaneously, including modern equations of state and an own numerical solver for the arising differential-algebraic system of equations, and provides new methods for the calibration of parameters of the metal hydride storage, proton-exchange membrane electrolyzer and fuel cell as well as a metamodel-based approach for sizing optimization. As a demonstrator for the novel tool, a simulation model of a hydrogen lab is successfully set up based on experimental results. The novel tool is able to extract polarization and jump curves of the fuel cell, determine a first temperature and pressure dependency of the efficiency of the electrolysis coupled with the metal hydride storage and speed up sizing optimization through metamodeling by a factor 262.1 at 4.9% and 32.7 at 3.3% accuracy.

## 1. Introduction

Power-to-Gas-to-X (PtGtX) systems are intensely discussed for a broad range of applications. For instance, [1] performs a technical review and [2] a techno-economic discussion including social and political aspects. In particular, systems consisting of photovoltaic (PV) cells, proton-exchange membrane (PEM) electrolysis, hydrogen storage based on metal hydrides, PEM fuel cells and buffer batteries (hybrid energy storage systems, HESS) are considered. These could be used to meet heat and electricity demands of homes, businesses, or small districts. However, the actual size of the individual components and their interplay are crucial for the technical and economic feasibility for the respective application [3]. Specifically, the system-internal heat exchange must be optimized. Systems partially consisting of the components mentioned above are analyzed in the literature. For instance, [4] discusses a mobile application, based on an experimental setup. An-

other study [5] reviews literature on HESS systems to provide insight into future directions and applications.

An essential tool to analyze and optimize such systems efficiently is an appropriate simulation model. Several simulators are already available for solving energy systems consisting of heat and power plants, renewable energy systems, electrical power, gas and district heating networks, as well as large and small energy consumers. Currently, there are hardly any software tools available that can simulate and efficiently optimize power, fluid and heat flows of such systems simultaneously.

Such a system can principally be simulated with plain MATLAB as has been indicated in [6]. However, their model for the area of the Aegean Sea uses simplified equations for alkaline electrolyzers, does not describe fuel cells, and heat recovery is not considered.

MATLAB *Simscape* with its *Specialized Power Systems* library contains a generic battery model, a PEM electrolyzer, and a PEM fuel cell stack [7]. However, simulation runs are slow, according to [8] for

\* Corresponding author.

E-mail address: [michael.bareev-rudy@h-brs.de](mailto:michael.bareev-rudy@h-brs.de) (M. Bareev-Rudy).

**Nomenclature****Acronyms**

CDL	Charge Double Layer
DAE(s)	Differential-Algebraic Equations (System)
DoE	Design of Experiments
EL	Electrolyzer
EOS	Equation of State
FC	Fuel Cell
GERG	European Gas Research Group
GSSEM	Generalized Steady-State Electrochemical Model
HES	Hybrid Energy Storage System
HG	Hydrogen Generator (= Electrolyzer)
IAPWS	International Association for the Properties of Water and Steam
iSOC	Initial State of Charge
LHS	Latin Hypercube Samples
MAD	Median Absolute Deviation
MEgy	Multiphysical Energy System Simulator
MHS	Metal Hydride Storage
MMAD	Mean of Median Absolute Deviations
MOO	Multi-Objective Optimization
MYNTS	Multiphysical Network Simulator
NEL	New Energy Lab
NSGA	Non-dominated Sorting Genetic Algorithm
PEM	Proton-Exchange Membrane
PtGtX	Power-to-Gas-to-X
PV	Photovoltaic
RBF	Radial Basis Function
ROW	Rosenbrock-Wanner Method
SOC	State of Charge

**Symbols**

$A$	Area of Respective Device ( $m^2$ )
$C$	Concentration (mol)
$C_{CDL}$	Capacity of Charge Double Layer (F)
$C_t$	Total Heat Capacity (J/K)
$c_p$	Specific Heat Capacity (J/(kg K))
$c_{LHV}$	Lower Heating Value (Wh/m <sup>3</sup> )
$D$	Diameter of Pipe (mm)
$D_{fc}$	Factor for Max. Achievable Stack Voltage
$e$	Specific Energy (J/kg)
$f$	Partial Derivates
$H_t$	Total Heat Transfer Coefficient (W/K)
$h$	Specific Enthalpy (J/kg)
$I$	Current (A)
$I_0$	Cell Exchange Current Density (A/m <sup>2</sup> )
$I_L$	Limiting Current (A)
$I_{stack}$	Current Through Stack (A)
$I_{load}$	Load Current (A)
$J$	Jacobian

$K_T$	Auxiliary parameter for optimization
$L$	Length of Pipe (mm)
$M$	Molar Mass (g/mol)
$m$	Mass (g)
$n_{cells}$	Number of Cells
$\dot{m}$	Mass Flow (g/s)
$P$	Power (W)
$p$	Pressure (bar)
$\dot{q}$	Measured Hydrogen Flow Rate (m <sup>3</sup> /h)
$R_{el}$	Electrical Resistance ( $\Omega$ )
$R_i$	Internal Resistance ( $\Omega$ )
$T$	Temperature (K)
$U_{act}$	Activation Voltage (V)
$U_{conc}$	Concentration Voltage (V)
$U_{Nernst}$	Nernst Voltage (V)
$U_{ohmic}$	Ohmic Voltage (V)
$U_0$	Reversible Cell Voltage (V)
$U_{stack}$	Stack Voltage (V)
$v$	Velocity
$x_i$	Iteration Vector
$y_k$	Experimental Results
$z$	Compressibility Factor

**Greek symbols**

$\alpha$	Charge Transfer Coefficient
$\eta$	Efficiency
$\lambda$	Friction coefficient of Pipe
$\rho$	Density
$\sigma$	Parameter of RBF multiquadric kernel
$\varphi$	Angle of Slope
$\xi$	Molar Fraction

**Subscripts**

$H_2$	Hydrogen
$O_2$	Oxygen
$avg$	Average
$e$	Edge
$est$	Estimated
$f$	From
$ref$	Reference
$t$	To

**Physics constants**

$F$	Faraday Constant (96 485.3415 C/mol)
$g$	Standard Gravity (9.806 65 m/s <sup>2</sup> )
$R$	Universal Gas Constant (8.314 462 J/(K mol))

energy system models of comparable complexity, and neither the numerical solver (see [9]) nor the event management (see [10]) can be controlled and reworked in all relevant aspects in order to improve numerical stability, performance and modeling of the energy management.

The Modelica-based *TransiEnt* library [11] for integrated energy systems (electricity, gas, heat) uses a similar mathematical model. However, simplified models are used for gas transport, electrolyzers and their thermodynamics. Although heat and power plant models are available, systems based on fuel cells and hydrogen storage seem to be missing. The focus is more on a dynamic system model that is suitable for the analysis of dynamic interactions of subsystems and the development of necessary resilience strategies.

*pandapipes* [12] is a network calculation program designed to automate the analysis of district heating and gas systems. *pandapipes* and the power systems calculation program *pandapower* can be used in combination to analyze multi-energy networks. An environment

capable of coupling both tools is pandapowerpro. pandapipes is based on isothermal Euler equations and only basic thermodynamic models of compressors. So far, electrolyzers, hydrogen storage, and fuel cells are missing. pandapipes is aimed at static analysis of balanced fluid systems. This allows analysis of static or quasi-static analyses of pressure and velocity distributions in fluid networks using incompressible or compressible media. Gas composition is assumed to be fixed. Alternatively, static or quasi-static analyses of temperature distributions in fluid networks can be conducted. Currently, this type of analysis is only possible for incompressible media.

For simulation and analysis of large energy networks, a software called MYNTS (MultiPhysical NeTwork Simulator, e.g. [13]) is developed. For gas transport networks, it solves transient non-isothermal Euler equations with advanced models for compressor thermodynamics and mixing of currently 21 gas components. MYNTS uses a semi-coupled approach; isothermal Euler equations (Eqs. (2), (3) below) are iterated with equations for enthalpy (Eq. (4) below, reformulated in terms of specific enthalpy) and gas composition. The equation of state (EOS) enters there. The modern standard GERG-2008 [14] for gases is used. However, a library for liquids such as IAPWS for water [15] is not included. For liquids, incompressibility is assumed in MYNTS. The respective system of equations is described in [16] for the case of water-based cooling (or heating) circuits including heat exchangers and, with the focus on its numerical solution, in [17]. In [13] an extensive literature review of simulators similar to MYNTS is carried out, showing that MYNTS contains all relevant modern features for gas transport simulation. MYNTS employs characteristic maps or profiles for elements such as compressors, electrolyzer plants, and fuel cell plants. However, for the level of detail considered here, such elements have to be modeled in more detail. An energy management suitable for a HESS such as the multi-stage energy management control introduced in [18] is not included so far.

For the level of detail considered here, each decisive component of the system has to be described by a set of differential(-algebraic) equations (DAEs). In [4] metal hydride storages (MHS) are analyzed and optimized based on experiments. Another study [6] describes a numerical model of an MHS. In [19] a more detailed model is analyzed experimentally and numerically. Pressurized gas tanks are discussed in [20]. Modeling and parameter identification of electrolyzers is reviewed and extended in [21]. A typical steady-state electrochemical model for fuel cells is described in [22] and further discussed in [23]. Another study [24] introduces a generalized steady-state electrochemical model. Similar dynamic models, adding the charge double-layer (CDL) effect, are described in [25,26]. In [23] several methods for calibrating parameters of a fuel cell (called regression there) are briefly reviewed. They are based on genetic algorithms, artificial neural networks, artificial bee colony, harmony search, whale optimization, and some hybrid formulations. However, they do not employ the known model equations. In addition, a mathematical analysis of the optimization problem itself, redundancies and possible reductions are not carried out.

In [27] it is shown that a set of partial differential-algebraic equations arises for the models discussed here. After its typical semi-discretization, a system of differential-algebraic equations (DAEs) remains to be solved. Rosenbrock-Wanner (ROW) methods have shown very good performance in benchmarks concerning DAE problems arising in energy network simulation [17]. In addition, Rodas5P is well suited for semi-discretized partial differential equations, and is one of the most efficient solvers in the family of ROW methods [28].

For optimal sizing of the components and development of an optimal control strategy for its operation, simulation-based optimization is standard in computer-assisted engineering. However, for the optimization of more than one criterion (multi-objective optimization, MOO), a standard workflow does not exist. Examples of different approaches for MOO are presented in [29] (genetic NSGA-II algorithm) for a reciprocal engine, in [30] (NSGA-II based on a cascade-forward neural network

with the Levenberg-Marquardt training method) for a solar thermal power plant, and in [31] (multi-objective mixed integer nonlinear programming coupling maximum rectangle method and particle swarm optimization) for capacity programming and operation optimization of a hydrogen-storage system for energy communities.

Such approaches typically require large series of simulation runs. Hence, they suffer considerably if the average run-time for a simulation run is high. The standard approach to overcome this limitation is metamodeling based on a thin experimental design. A metamodel is a “model of a model”, meaning that it ideally reproduces the same outputs for the same inputs as the original model, while being significantly faster to compute. It is constructed based on a data set of samples of the original model by means of a mathematical approximation process. Metamodels are then able to approximate outputs for inputs, which are not included in their constructing data set. The work [32] describes metamodel-based simulation optimization and reviews typical methods from machine learning. They involve the setup of appropriate thin experimental designs for such parameters of the simulation model which shall be optimized. Based on the respective samples of simulation results, a mathematical approximation is constructed. Several methods for the design-of-experiments as well as the approximation method are commonly used. Typical suggestions involve Gaussian kernels. That this can be suboptimal is shown in [33], particularly for applications considered here. Alternatives are analyzed regarding approximation quality and computation time.

In this paper, the multiphysical energy system simulation, analysis and optimization tool MEgy is introduced. MEgy models electrochemical and thermodynamic processes describing currents, voltages, pressures, mass and enthalpy flows inside and in-between the decisive components. The models of the specialized Power Systems library of MATLAB Simscape form a basis of the work described here. However, they are extended and coded in plain MATLAB in order to drastically speed up simulation runs and enable control on the numerical solver and the event management. In particular, Rodas5P, an own numerical solver for the arising differential-algebraic system of equations, is efficiently integrated.

The gas transport part of MEgy and MYNTS are based on the same set of equations. Besides GERG-2008 [14], IAPWS [15] is used additionally. MEgy resolves elements such as compressors, electrolyzer plants, and fuel cell plants in more detail compared to MYNTS.

Innovations with regard to the modeling include identification or calibration processes for parameters of two decisive subsystems, namely the hydrogen generation consisting of PEM electrolyzer plus metal hydride storage (MHS) and the PEM fuel cell, and an extended degradation model for PEM fuel cells. The novel parameter calibration process described below comprises selected experimental studies of the dynamic behavior and transient response, based on modified setups of [26], as well as a multistage optimization process of the model parameters. A multidimensional Newton method is used for solving respective optimization problems. The Newton method as such is not new, but its efficient application to the case considered here.

In order to facilitate the efficient solution of optimization tasks, a metamodeling approach is introduced, tailored to the problems considered here. The performance of the overall approach is demonstrated based on experimental results obtained in the hydrogen lab at the Hochschule Bonn-Rhein-Sieg (H-BRS; see affiliation of the authors). It is shown that the calibrated simulation model can approximate decisive operational scenarios for the production and consumption of hydrogen under various load jumps and temperature changes, providing a basis for the further development of energy management processes.

## 2. Methods

In this paper a workflow for metamodel-based simulation optimization is developed (see Figure A1). In the following, important building blocks of the workflow are explained: The constitutive equations of

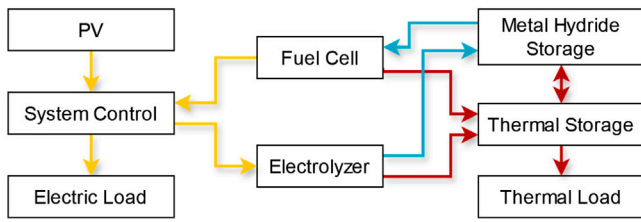


Fig. 1. Process flow diagram of PtGtX HESS. Arrows show flows: yellow for electrical power, blue for hydrogen, red for heat.

the mathematical model are summarized in Section 2.1, the main building blocks of the simulator are summarized in Section 2.2, the experimental setups and parameter calibration steps are explained in Section 2.3, with more details on the simulation scenario in Section 3, the metamodeling-based optimization is introduced and analyzed in Section 2.4. Note that actual optimizers for tasks such as optimal sizing of components are out of scope of this paper.

## 2.1. Mathematical model

A PtGtX system consists of several components that form a network (see Fig. 1). Each component is described by means of a mathematical model consisting of one or more equations describing a pure electrical subnet, an electrochemical system, or a fluid transport subnet including its thermodynamics. The components are connected using Kirchhoff's junction and loop rules.

### 2.1.1. Underlying graph model

In order to provide a general description of such a network, the components are expressed in terms of nodes and directed edges: Nodes contain state variables, i.e. a potential, while edges contain process variables, i.e. a flow. When an edge is connected to two nodes, it is exposed to the difference in potential between them. The flow between these nodes, i.e. the flow through the edge, is calculated as a function of the difference in potential. An edge is defined to have a "geometrically" positive direction to take into account the direction of flow: if the flow is in the direction of the edge, then it has a positive sign. Otherwise, the sign is negative. A node is either set to given potentials and thus acts as a source or sink for a flow, or it balances the incoming and outgoing flows of the connected edges. The node's potentials are then determined by the network's system of differential-algebraic equation. Differential equations are used to model components that are assigned a storage function, such as a battery or gas tank.

### 2.1.2. Electrical network model

In an electrical network, nodes have the state variable voltage  $U$ . An electrical component (edge) calculates the current  $I$  through it as a function of the voltage difference across it. In the case of a simple resistor, the equation is

$$I_e = \frac{U_f - U_t}{R_{el}} \quad (1)$$

where  $I_e$  is the current,  $U_f$  and  $U_t$  are the voltage potentials of the connected nodes and  $R_{el}$  is the resistance value. The subscripts  $f$  for "from" and  $t$  for "to" denote node variables according to where a connected edge starts or ends. The subscript  $e$  denotes the flow variable of the edge. Similarly, more complex components can be implemented, such as diodes, batteries, power supplies, voltage converters, photovoltaics, etc.

### 2.1.3. Fluid transport model and its thermodynamics

In the part of the energy network which describes transport of fluids (e.g. water, hydrogen, oxygen), nodes have two state variables: the pressure  $p$  and specific enthalpy  $h$ . Each edge has a mass flow  $\dot{m}$  attached. In the following, the governing equations used are outlined.

The Euler equations are a system of nonlinear hyperbolic partial differential equations. In time  $t$  and (one-dimensional) space  $x$  for gas flowing through a pipe, they read [13]

$$\frac{\partial \rho}{\partial t} + \frac{\partial}{\partial x}(\rho v) = 0 \quad (2)$$

$$\frac{\partial}{\partial t}(\rho v) + \frac{\partial}{\partial x}(p + \rho v^2) = -\frac{\lambda}{2D} \rho v |v| - \rho g \sin(\varphi) \quad (3)$$

$$\frac{\partial}{\partial t} \left( \rho \left( \frac{v^2}{2} + e \right) \right) + \frac{\partial}{\partial x} \left( \rho \left( \frac{v^2}{2} + e \right) v + p v \right) = r_s \quad (4)$$

with  $\rho = \rho(x, t)$  being the density,  $p = p(x, t)$  the pressure,  $e = e(x, t)$  the specific energy,  $v = v(x, t)$  the velocity of the gas,  $\varphi$  the angle of slope,  $D$  the diameter of the pipe,  $\lambda$  the friction coefficient,  $g$  the gravitational constant,  $r_s$  a term modeling heat exchange with the surroundings of the pipe, and  $m$  the mass. Note that the pressure gradient due to friction along a pipe section of length  $L$  is modeled by the Darcy-Weisbach equation for pipes [34]:

$$\Delta p = \frac{\lambda L}{2D} \rho |v| v \quad (5)$$

Several models exist for computing  $\lambda$ , depending on whether the fluid flow is laminar (Hagen-Poiseuille), turbulent (e.g. Nikuradze) or in between. For more details, refer to [34]. An additional equation is necessary in case of compressible fluids:

$$p = T \rho \frac{R}{M} z \quad (6)$$

with  $T = T(x, t)$  being the temperature,  $z = z(p, T)$  the compressibility factor,  $M$  the molar mass of the fluid, and  $R$  the universal gas constant. Eq. (4) can be reformulated in terms of the specific enthalpy  $h = e + \frac{v^2}{\rho}$ .

The velocity can be replaced by means of  $v = \frac{\dot{m}}{\rho A}$  with  $A$  being the cross section of the pipe (assumed to be constant for each pipe segment). Eq. (6) is used to replace  $\rho$ . Overall, MEgy solves for  $p$ ,  $\dot{m}$ ,  $h$ . In order to convert between enthalpy and temperature, a typical approximation is used:

$$h = c_p \cdot T \quad (7)$$

with  $c_p = c_p(p, T)$  being the specific heat capacity, also computed by the EOS. A so-called equation-of-state (EOS) for fluids is necessary to obtain thermodynamic properties of the fluids (in both, the compressible and incompressible case) including  $z$ . More details can be found in the following section. In case of incompressible fluids, i.e.  $\frac{\partial \rho}{\partial t} = \frac{\partial \rho}{\partial x} = 0$ , the so-called water-hammer equations can be used [17].

### 2.1.4. Equations of state

In order to compute the thermodynamic properties of the different fluids hydrogen, oxygen, water (liquid), and water vapor, appropriate equations of state modeling real fluid behavior are necessary. The GERG-2008 equation of state [14] has a much more complex description than typical virialtype equations. Here, the compressibility factor  $z$  is modeled based on the Helmholtz free energy, split into parts for ideal and residual fluid. A large amount of measurement data for different combinations of fluids is used to fit the considerable number of coefficients. Details can be found in [14] and ISO 20765-2/3. From the current pressure  $p$ , temperature  $T$ , and gas composition expressed by means of its vector of mole fractions  $\xi$ , first the molar density  $\rho_m$ , then the compressibility factor  $z$  and the enthalpy  $h$  are computed. Thus, Eq. (6) is an implicit function for pressure  $p$ . Since GERG does not compute appropriate values for water, particularly for the liquid and the mixed liquid-vapor phase, the IAPWS-95 model [15] is used instead.

### 2.1.5. Metal hydride storage model

For a metal hydride storage tank, a 0D model [19] with conservation equations based on the ones reported in [17] is used. The change of mass of the solid phase (alloy-hydride phases) is calculated by applying the mass conservation law, and the mass flow between the gas and the solid phase is modeled by specific reaction terms based on the Arrhenius equation with constants for absorption and desorption reaction rates and the equilibrium pressure, which is often described by the van't Hoff equation [35]. For the FeTiMn metal hydride storage in use the pressure composition isotherm described for a similar tank and FeTiMn alloy in [36] is utilized. In order to calculate the change of energy and thus the associated temperature of the solid phase (hydride and gas phase together), the energy conservation equation is applied. For more details on the activation and thermal management of multiple tanks, see [19].

### 2.1.6. Electrochemical models

Since the parameter calibration process for the fuel cell stack requires partial derivatives of the governing equations, these are discussed in detail. The electrochemical model of the PEM electrolyzer is introduced in its rudimentary form, as the electrolyzer in the experimental setup considered in this paper is used for a constant power in a quasi-static operating mode, with only slow changes due to the attached MHS. Nevertheless, a detailed model together with an intense discussion of the parameters involved and an appropriate fitting process is discussed in [21]. This approach is implemented into MEgy.

**Fuel cell model.** As for the PEM fuel cell, electrochemical parts of the model are based on the Nernst equation, Butler-Volmer equation and typical assumptions for simplifications of the reaction kinetics. According to [23] for  $T < (273.15 + 100)$  K:

$$\begin{aligned} U_{stack} &= n_{cells} \cdot (U_{Nernst} - U_{act}(I) - U_{ohmic}(I) - U_{conc}(I)) \\ U_{Nernst} &= 1.229 - (T - T_{25}) \frac{44.43}{2F} + \frac{RT}{2F} \ln(p_{H_2} \cdot p_{O_2}^{0.5}) \\ U_{act}(I) &= \frac{RT}{2\alpha F} \ln(I/I_0) \\ U_{ohmic}(I) &= \frac{I}{A} \cdot R_i \\ U_{conc}(I) &= -B \ln(1 - \frac{I}{I_L}) \end{aligned} \quad (8)$$

with  $n_{cells}$  being the number of cells in the stack,  $T_{25} = 298.15$  K,  $F$  the Faraday constant,  $U_{Nernst}$  being the thermodynamic potential of the cell that represents its reversible voltage (Nernst voltage),  $U_{act}$  the Tafel equation for the activation overvoltage (voltage drop), with  $I_0$  the cell exchange current, and  $\alpha$  (charge transfer coefficient) being an unknown parameter of the cell to be retrieved via calibration,  $U_{ohmic}$  the ohmic overvoltage, and  $U_{conc}$  the concentration overvoltage resulting from the transportation of the reacting gases, with  $I_L$  being the limiting current and  $B$  as another unknown parameter of the cell to be retrieved via calibration. Models for the partial pressures  $p_{H_2}$  of hydrogen and  $p_{O_2}$  of oxygen can be found in [23] as well. An alternative for the Tafel equation would be

$$U_{act,GSSEM}(I) = -(\xi_1 + \xi_2 \cdot T + \xi_3 \cdot T \cdot \ln(C_{O_2}) + \xi_4 \cdot T \ln(I)) \quad (9)$$

with  $C_{O_2}$  being the oxygen concentration at the membrane/gas interface of the cathode

$$C_{O_2} = \frac{p_{O_2}}{5.08e6 \cdot \exp(-498/T)} \quad (10)$$

and  $\xi_1, \dots, \xi_4$  unknown parameters to be retrieved via calibration.  $U_{act,GSSEM}$  is the so-called generalized steady-state electrochemical model (GSSEM) for a PEM fuel cell [24].

A dynamic model of the stack adds two equations, one for the charge double layer (CDL) effect and another one for the thermodynamic response. A simple equivalent circuit with a capacitor modeling the CDL

is described e.g. in [26]. In [25] a slightly extended model is presented:

$$\frac{dU_{act}}{dt} = \frac{I}{C_{CDL}} - \frac{U_{act}I}{(U_{act,0} + U_{conc})C_{CDL}} \quad (11)$$

with  $C_{CDL}$  modeling the CDL. The change of the temperature of the cell is modeled by

$$C_t \frac{dT}{dt} = I(U_{act} + U_{ohm} + U_{conc}) - H_t(T - T_{ref}) \quad (12)$$

with  $C_t$  being the total thermal capacitance,  $H_t$  the total heat transfer coefficient, and  $T_{ref}$  the reference temperature.

**Degradation model for fuel cells.** For PEM fuel cells, an extended degradation model is developed. A typical model [37] is used as a basis. It considers start/stop, idling, load changes, and high power scenarios. In the case of targeted operation only in the medium power range, the fuel cell would age only during the on/off switching processes. Therefore, the degradation model is extended by an aging at nominal load. It produces a factor  $D_{fc}$  for the maximal achievable stack voltage  $D_{fc} U_{stack}$ . Details can be found in [8].

**Electrolyzer model.** The PEM electrolyzer model depends on the Nernst equation and Butler-Volmer equations as well:

$$U_{stack} = n_{cells} \cdot (U_{Nernst} + U_{act}(I) + U_{ohmic}(I) + U_{conc}(I)) \quad (13)$$

In contrast to the fuel cell however, the cell voltage increases with rising current. The electrochemical model of the PEM electrolyzer, together with a detailed discussion of the parameters involved and different models for them, is discussed in [21].

## 2.2. Multiphysical energy system simulator

In order to solve the mathematical model described above, a novel simulator called MEgy (Multiphysical Energy System Simulator) is developed. It is implemented in an object-oriented manner in plain MATLAB instead of MATLAB Simulink Simscape, which provides increased performance and allows for flexibility and extensibility. To be more specific, numerical tests for an energy system model of a hydrogen ferry of comparable complexity to the HESS considered here reveal a speedup factor of approximately 3 if MATLAB is used instead of MATLAB Simulink Simscape [8]. The event management and the numerical solver can be improved considerably if MATLAB is used instead of Simscape as numerical experiments in [9,10] demonstrate for energy systems consisting of electrolyzers, fuel cells and batteries on the basis of Simscape models. The goal is the ability to use many simulation models as building blocks to create an interconnected system or network. MEgy is designed to be flexible and extendable by supporting the addition of custom models, referred to as components. Based on a description of such a network, MEgy automatically creates the algebraic-differential system of equations, mass matrix, Jacobian sparsity pattern, etc. that are used by a numerical solver to simulate the network. For more details on the structure and operation of MEgy, see Appendix B.

### 2.2.1. Problem type

All equations can be summarized into a system of differential-algebraic equations (DAEs) of type

$$M y' = f(t, y), \quad y(t_0) = y_0 \quad (14)$$

where  $y = y(t)$  is the state vector of the system to be calculated. In most cases  $M$  is a singular diagonal matrix with entries zero defining algebraic equations and one defining differential equations. Even if pipes are considered and modeled via partial differential equations, a suitable semi-discretization in space leads to a DAE problem of type (14) [27]. The index of the DAE system (14) is assumed to be one, thus many standard DAE solvers can be applied. In order to solve the equations, consistent initial values  $y_0$  fulfilling the algebraic equations must be provided.

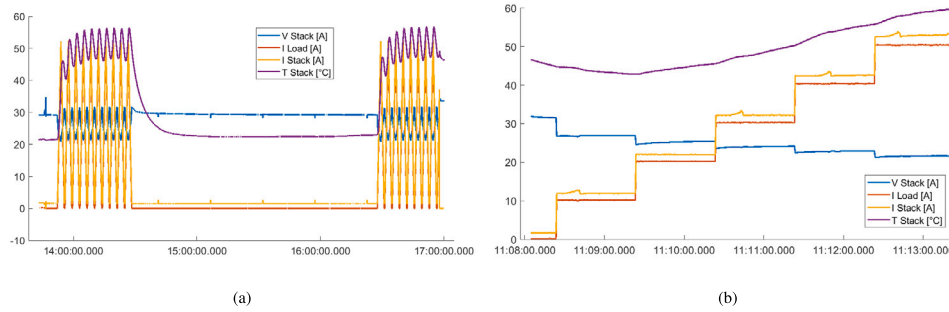


Fig. 2. Load profiles and experimental results for analyzing the polarization curve of the fuel cell. The load-dependent regular purging of the stack is clearly visible in (b).

MEgy interacts with the numerical solver through the standard MATLAB interface by providing it with an internal method. However, the handling of events has been modified compared to the standard MATLAB solver. This simplifies the restart of the solver after control measures, which often occur in these simulations. The solver passes the current state vector  $y(t)$  to the method, which is then able to compute the right-hand side  $f(t, y)$  of the DAE system (14).

### 2.2.2. Numerical solver

In MEgy a MATLAB implementation of the Rodas5P solver [28] is applied for problem (14). Rodas5P is a fifth order Rosenbrock-Wanner (ROW) method for solving index one DAEs. Compared to fully implicit methods, ROW schemes are easy to implement and avoid the solution of non-linear equations. However, Jacobian information is included in their formulation and must be calculated within each time step. Nevertheless, ROW methods have shown very good performance in benchmarks concerning DAE problems arising in energy network simulation [17]. In addition, Rodas5P is well suited for semi-discretized partial differential equations, and is one of the most efficient solvers in the family of ROW methods [28].

In order to compute consistent initial values, a Newton iteration process is applied first to all algebraic equations included in system (14). Moreover, the handling of events has been modified compared to standard MATLAB solvers. This simplifies the restart of the solver after control measures. Such control measures very often take place in the network, e.g. to switch the electrolysis or fuel cell on or off.

## 2.3. Parameter calibration

In the following, the general experimental setup (Section 2.3.1) as well as two separate parameter identification or calibration processes with their setups are described. The parameter identification process for the electrolyzer cannot be separated from the time- and temperature-dependent behavior of the absorption process inside the MHS tanks. Therefore, Section 2.3.2 introduces a setup for their simultaneous analysis.

The calibration processes for the fuel cell stack comprise selected experimental studies of the dynamic behavior and transient response (Section 2.3.3) as well as a multi-stage optimization process of the model parameters (Section 2.3.4). First, the parameters of the quasi-stationary variant of the model of the respective component are optimized in order to approximate the typical characteristic curves. Afterwards, transient effects such as over- and undershooting and temperature dependencies are considered. A multidimensional Newton method is used for solving respective optimization problems.

### 2.3.1. General experimental setup

The system used for calibrating the simulation model is a Heliocentris New Energy Lab (NEL) [38] at H-BRS. It consists of a 1200 W PEM Nexa fuel cell with a Ballard FCgen 1020ACS stack [39], a 560 W PEM electrolyzer (Heliocentris PEM Hydrogen Generator Rack WM series by

Swissgrid) with a maximum flow rate of 1.2 NL/min (72 NL/h), three metal hydride storage tanks MHS 800 [40], an electronic direct-current load, buffer batteries, and a power management system. Measurements have a resolution of 0.5 s for experiments with the fuel cell stack and 1 s for experiments with hydrogen generation.

### 2.3.2. Experiments for the electrolyzer and metal hydride storage

The goals are to calibrate the reachable maximum power and corresponding efficiency of the subsystem and to approximate the pressure-temperature curve for use in simulation models of the entire PtGx system with its HESS.

The NEL electrolyzer operates at a constant, adjustable maximum pressure (16 bar). The resulting pressure of the hydrogen in the short pipe just before the storage tanks depends on both the temperature and the state of charge (amount of hydrogen absorbed) of the MHS. Since hydrogen absorption is an exothermic process, it is advantageous to cool the MHS tanks to slow the pressure rise and fill them in fewer cycles. This is aided by keeping the back door of the NEL hydrogen rack open during experiments. The room temperature is between 20.5 and 21.5 °C, and it would take several hours to completely cool the MHS between filling cycles.

For computing the efficiency  $\eta_{HG}$  of the hydrogen generation, the lower heating value  $c_{LHV}$  of  $H_2$  is necessary:  $c_{LHV} = 3000 \text{ Wh/m}^3$ . Then

$$\eta_{HG} = c_{LHV} \dot{q} / P_{HG} \quad (15)$$

where  $q$  is the measured hydrogen flow rate (converted from NL/min to  $\text{m}^3/\text{h}$ ), and  $P_{HG}$  the power obtained from multiplying measured current and voltage per time step. Note that the approximated efficiency of the PEM electrolyzer using its nominal flow rate and nominal maximum power is  $72 \text{ NL/h} \cdot c_{LHV} / 560 \text{ W} = 0.3857$ .

### 2.3.3. Load profiles for the fuel cell stack

Basic load curves for producing experimental data to calibrate the polarization curve are shown in Fig. 2(a) and, in more detail, in Fig. 3. The basic load profile which is repeatedly used for producing experimental results for the dynamic response to jumps of 10 A each is shown in Fig. 2(b). Note that load jumps must last long enough for the voltage to reach a stable level before increasing or decreasing the load current again, as shown in [26]. Experimental setups described in [38] with jumps every 20 s do not fulfill this condition. However, for the system at hand it is sufficient to wait 60 s after a jump, in contrast to the approx. 500 s used in [26] for a comparable, but older Nexa fuel cell stack. This drastically reduces the energy consumption of the experiments.

### 2.3.4. Multidimensional Newton method

The NEL system cannot operate in the concentration polarization region where gas transport losses occur. Hence,  $U_{conc} = 0$  is used. In the following,  $U_{act}$  is used instead of  $U_{act,GSSSEM}$  since less parameters

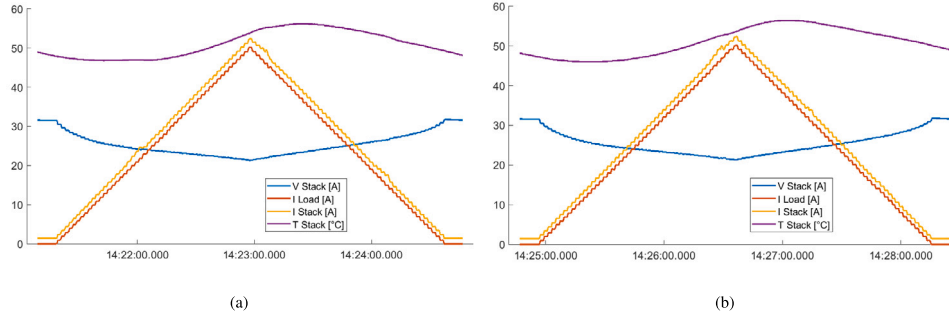


Fig. 3. Load profiles for analyzing the polarization curve of the fuel cell: two typical examples (run 9 (a) and run 10 (b)) after warming up. Experimental results are shown as well.

have to be calibrated, and these parameters offer direct physical interpretation (see also Section 3.2). The stack voltage model then depends on  $I$  and  $T$  as well as the parameters  $\alpha$ ,  $I_0$ , and  $R_i$ . Let  $K := \frac{R}{\alpha F}$ . It follows

$$U_{stack} = U_{stack}(I, T, K, I_0, R_i) \quad (16)$$

The model shall be calibrated by optimizing values of these parameters.

Let  $U_{stack}(I_k) = U_{stack}(I_k, T, K, I_0, R_i)$  and  $\{(I_k, y_k)\}$  a set of experimental results where  $U_{stack}(I_k)$  shall approximate  $y_k$ . The following minimization task has to be solved

$$F_{min} = \sum_{k=1}^n (U_{stack}(I_k) - y_k)^2 \quad (17)$$

The multidimensional Newton method for that task reads

$$J(x_{i+1} - x_i) = -f(x_i) \quad (18)$$

with  $f$  being the partial derivatives of  $F_{min}$  with regard to the parameters,  $x_i$  the iteration vector of unknown parameters and  $J$  the Jacobian of  $f$ .  $f$  is defined by Eq. (19) resp. Eq. (20) below. Two cases are considered.

**Case 1 – fixed temperature.** In the first case,  $T$  is fixed to the average temperature  $T_{avg}$  obtained during experiments. With  $K_T := T_{avg} \frac{R}{\alpha F}$  the following parameters have to be optimized:  $K_T$ ,  $I_0$ ,  $R_i$ . More precisely, the following set of conditions is obtained:

$$\begin{aligned} \text{Since } \frac{\partial}{\partial K_T} U_{stack} &= \ln\left(\frac{I}{I_0}\right) : & \sum_{k=1}^n (U_{stack}(I_k) - y_k) \cdot \ln\left(\frac{I}{I_0}\right) &= 0 \\ \text{Since } \frac{\partial}{\partial I_0} U_{stack} &= -\frac{K_T}{I_0} \cdot \ln(I) : & \sum_{k=1}^n (U_{stack}(I_k) - y_k) \cdot \frac{K_T}{I_0} \cdot \ln(I) &= 0 \\ \text{Since } \frac{\partial}{\partial R_i} U_{stack} &= \frac{I}{A} : & \sum_{k=1}^n (U_{stack}(I_k) - y_k) \cdot \frac{I}{A} &= 0 \end{aligned} \quad (19)$$

**Case 2 – variable temperature.** In the second case,  $T$  represents the temperature measured during experiments. Instead of using Eq. (12), the temperature dependency can here be described by a polynomial calibrated by means of the experimental results. Hence, the parameters  $K$ ,  $I_0$ ,  $R_i$  remain to be optimized. More precisely, the following set of conditions is obtained:

$$\begin{aligned} \text{Since } \frac{\partial}{\partial K} U_{stack} &= T \cdot \ln\left(\frac{I}{I_0}\right) : & \sum_{k=1}^n (U_{stack}(I_k) - y_k) \cdot T \cdot \ln\left(\frac{I}{I_0}\right) &= 0 \\ \text{Since } \frac{\partial}{\partial I_0} U_{stack} &= -\frac{T \cdot K}{I_0} \cdot \ln(I) : & \sum_{k=1}^n (U_{stack}(I_k) - y_k) \cdot \frac{T \cdot K}{I_0} \cdot \ln(I) &= 0 \\ \text{Since } \frac{\partial}{\partial R_i} U_{stack} &= \frac{I}{A} : & \sum_{k=1}^n (U_{stack}(I_k) - y_k) \cdot \frac{I}{A} &= 0 \end{aligned} \quad (20)$$

### 2.3.5. Estimation of stack current and power correction

In order to apply the obtained polarization curve, the resulting current  $I_{stack}$  of the fuel cell stack as a response to the current  $I_{load}$  of the load has to be estimated. For this purpose, the deviation of  $I_{dev} = I_{stack} - I_{load}$  is measured for each 10 A-jump experiment.  $I_{dev}$  contains responses to purging steps, which are removed by applying MATLAB's `filloutliers` with the options ('linear', 'movmedian', 100), followed by `smoothdata` with the options ('movmedian', 100). The window size 100 corresponds here to 50 s. Averaging over the values per time step of all 10 A-jump experiments forms the  $I_{dev,est}$  estimation. Then  $I_{stack,est} = I_{load} + I_{dev,est}$ .

Note that the CDL is indirectly taken into account here. The experimental results shown in Fig. 2(b) represent a CDL, but the undershooting for the steps upwards (as well as the overshooting for steps downwards) is small due to the resolution of the measurement equipment of the NEL, so that explicit fitting of  $C_{CDL}$  is dropped. In addition, a power correction factor is computed to check the deviations of the accumulated power consumption for a 10 A-jump experiment and its estimated curve.

### 2.4. Metamodel-based simulation optimization

MEgy is used to construct a simulation network composed of the calibrated fuel cell, electrolyzer, metal hydride storage and battery to simulate a hybrid energy storage system akin to the hydrogen lab at H-BRS (see Fig. 1). The goal is to use metamodel-based simulation optimization in order to find the optimal sizing of the components for a given scenario. A scenario in this case is defined as the combination of electrical load and PV production profiles, for a time span of typically 24 h. Metamodel-based optimization is used, because a simulation of 24 h of a scenario takes about 30 s. The sizing is determined by optimizing over a whole year. Due to a simulation time of 30 s for a 24 h simulation and thus a simulation time of 3 h for a simulated year, it is not feasible to use direct simulation optimization. With the iterative process of optimizers, they converge unacceptably slowly on a suitable solution, if every step of the optimization takes this long. If approximately 1000 iteration steps are required to find an acceptable solution, even with the parallel function evaluations on 8 cores of the utilized optimizer, it would still require about 15 days of simulation (see Fig. 4). Instead, a "thin data" approach is used: the HESS is simulated for 24 h in varying configurations for the component sizing for representative days by using Design of Experiments. Because the simulations are not sequential, i.e. not dependent on previous ones, parallel processing is used to significantly decrease the required time for all simulations. From the simulation results, the time series of each component's power is reduced to the consumed (or stored) or produced (or released) energy over the simulated time period through integration. This results in outputs for a specific set of inputs, which represent discrete points in the multidimensional parameter space. In order to be able to optimize continuously over these discrete points,

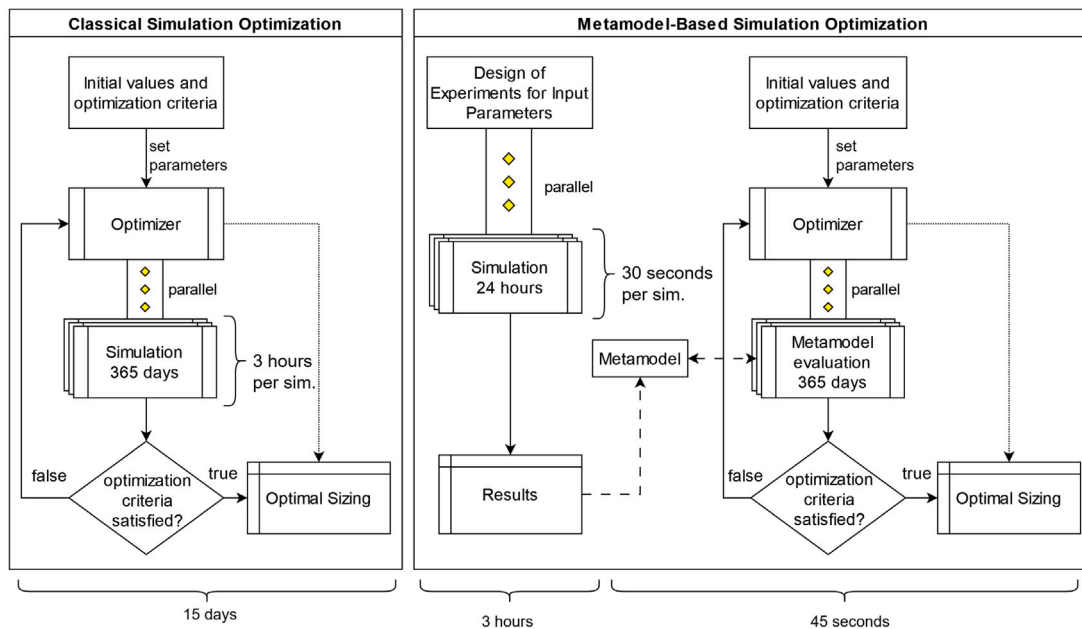


Fig. 4. Comparison of required time for classical and metamodel-based simulation optimization. Calculations assume parallel processing on 8 cores and a DoE with 256 samples for each of 9 representative days.

a metamodel is employed, which approximates outputs outside the original simulation results. The metamodel is used to approximate the component's energy balance and SOCs of one day, which is in turn used as a starting point for the next day. This approach is used to estimate the behavior of the system for a whole year for the given sizing. It can then be used to find a Pareto front for the desired optimization criteria (see Figure A1). The trade-off of such a metamodel is lower accuracy with drastically increased speed.

**Radial basis function.** For the metamodel, radial basis functions (RBF) are used due to their ability to reproduce nonlinear behavior and their relatively low computational complexity [33]. The multiquadric kernel function is selected for the RBF, which has a parameter  $\sigma$  that is recommended to be set between 0.1 and 0.5. However, this parameter can be optimized to tune how well the RBF reproduces the underlying data structure. For this, the MATLAB function `fminsearch` is used to minimize the deviation between the metamodel outputs and simulation outputs that are not included in the constructing dataset.

**Design of experiments.** With the power or capacity of every component being an independent input parameter, it results in a multidimensional input space, which needs to be traversed in a systematic way. Here, the 8 input parameters are the capacity and initial state of charge (iSOC) of the battery and MHS, the maximum power of the electrolyzer and fuel cell, and scalars for the load and PV profiles. Design of Experiments (DoE) is used to create a space-filling sampling plan, which is then used to vary the power and size of the components and run simulations for a given scenario. In [33] it is shown that for a lower number of samples (up to 2000) RBF metamodels created from Sobol samples perform better than those from Latin hypercube samples (LHS). An additional advantage of Sobol samples is their extensibility, which is why they are chosen in this application.

### 3. Results and discussion

In the following, results obtained with the novel parameter calibration processes, the overall simulation model for the hydrogen lab and its metamodel are discussed.

#### 3.1. Parameter calibration for the electrolyzer and metal hydride storage

Measured temperatures, pressures and flow values can be found in Figs. 5 and 7, showing the typical pressure–temperature correlations with a clear dependence on the starting temperature of the conducted experiment. The cool-down phase is between ca. 12:00 and 13:00. Note that the NEL's nominal maximum flow rate of 1.2 NL/min is not reached. Between 1.10 and 1.15 NL/min are realistic.

As can be seen from the exemplary two runs of the electrolyzer shown in Fig. 7, the pressure–temperature dependence exhibits an expected behavior, cf. [38]: A steep increase, followed by a nonlinear increase with a moderately increasing derivative for a while, and a steeper ascend finally. The increase in temperature is substantial and cannot be neglected for an optimal energy management. It is, however, strongly dependent on the starting pressure as well as the temperature of the MHS, the electrolyzer and the surroundings, as can be seen from Fig. 5. Pressure and temperature are decreasing during the cool-down phase (the pressure in the pipe will see the decreased pressure in the tanks after reopening the valves), but the temperature more than the pressure. Hence, the shift of the pressure–temperature curve is to be expected. Therefore, simulations need to compute a starting point for both temperature and pressure if waste heat and/or heat management shall be considered.

Results for the reachable maximum power and corresponding efficiency  $\eta_{HG}$  of the NEL electrolyzer are shown in Figs. 6 and 8. The nominal maximum power of 560 W is hardly reached. The typical range is between 500 and 530 W with experimental history-dependent centers at around 500 W and 520 W. The efficiency is around the calculated nominal value (see Section 2.3.2), but varies substantially.

The range of efficiency values  $\eta_{HG}$  obtained from the experimental results, see Fig. 8, is around 0.38 and as expected a bit lower than the nominal value. The value 0.38 is used for the first simulation model of the HESS at H-BRS. However, Fig. 8 demonstrates a moderate dependency of  $\eta_{HG}$  from temperatures and pressures of the MHS and electrolyzer and the surroundings as well. Hence, a limitation of the current workflow is that a corresponding mathematical model reflecting this dependency could be set up, but is not used yet. By means of this model, a heat management could be introduced in order to keep temperature effects and waste heat as small as possible. Such

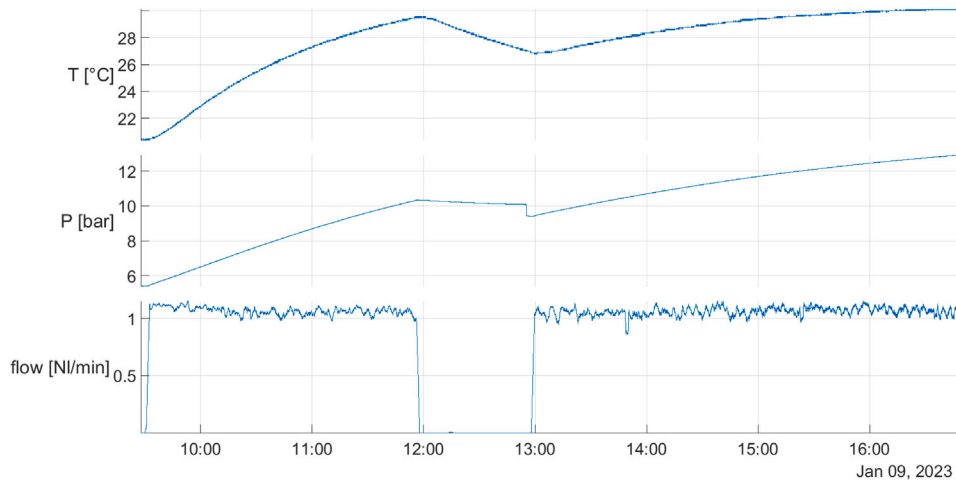


Fig. 5. Exemplary experimental results for hydrogen generation and absorption with a cool-down phase (zero flow) in between (one working day).

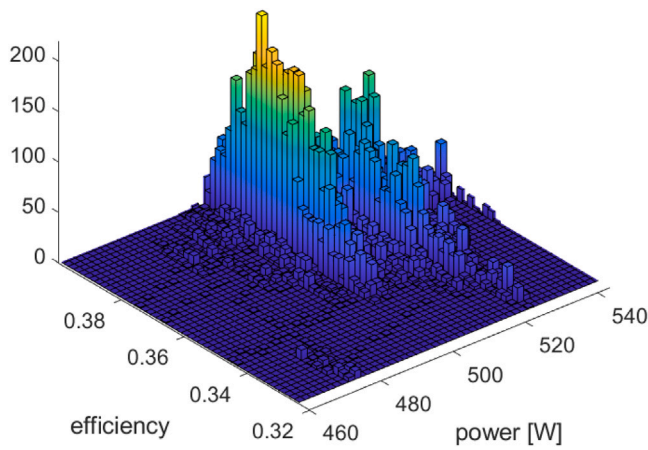


Fig. 6. 3D histogram of efficiency  $\eta_{HG}$  vs. power for the relevant part of Fig. 8(b).

a heat management will be necessary for the purposes of optimizing the general sizing and performance of HESS systems (cf. Section 3.3) further.

### 3.2. Parameter calibration for the fuel cell stack

Exemplary results of the experiments conducted are shown in Fig. 2(a) and, in more detail, in Fig. 3 for the calibration of the polarization curve. Experimental results showing the dynamic response to jumps of 10 A each are shown in Fig. 2(b). These data are used for the multidimensional Newton method described in Section 2.3.4, followed by the estimation of stack current and power correction, as described in Section 2.3.5.

As can be seen from Figs. 9(a) and 9(b), both cases for calibrating the polarization curve result in small errors of around 0.004 for Case 1, with a  $T_{avg}$ , and 0.003 for Case 2, with an approximation of the temperature curve. Resulting values for  $K$  are close, but for  $I_0$  and  $R_i$  not. Such situations have been reported in [23], for instance. From the mathematical calibration process, this has to be expected — even if these parameters have a physical meaning, a calibration process might end in parameter sets representing nonphysical optima. Note that more than one global optimum can exist for the optimization problem posed here, and the calibration might end in a (good) local optimum as well. This is a general problem found in calibration processes for fuel cells as well as electrolyzers [21].

Table 1

Statistics on correction factors for optimized dynamic behavior of step-up and step-down load profiles.

	Average corr. factor		Average deviation	
	$I_{stack,est}$	$I_{stack}$	$I_{stack,est}$	$I_{stack}$
Step-up	1.0131	1.0109	0.0023	0.0019
Step-down	1.0365	1.0365	0.0027	0.0021

As can be seen from Table 1 and Figs. 10(a) and 10(b), the power correction gives an improvement and is moderate. For the step-up part of the 10 A-jump experiments, the accumulated consumed power needs a correction of 1.31%, for the step-down part a correction of 3.65% on average. The standard deviation is small. Since overall power consumption is usually an important criterion, the correction is suggested.

As an alternative to  $U_{act}$ , the GSSEM model with  $U_{act,GSSEM}$  can be tried. Instead of three parameters, the four  $\xi_i$  values have to be optimized. As can be expected, the Newton method works, but results are not better in terms of residuals.

Working in the regime of  $U_{conc} = 0$  is beneficial for the calibration process since the additional parameter  $B$  can be left out of the optimization process. It could be fit afterwards if respective experimental results were available which is, however, not possible with the NEL system so far.

Since the undershooting and overshooting representing the CDL is small due to the resolution of the experimental data that can be obtained from the NEL, explicit fitting of  $C$  is not performed. If more accurate data are available,  $C_{CDL}$  can be also fit afterwards with all parameter values obtained so far acting as initial solutions to the optimization process.

### 3.3. Simulation model of the hydrogen lab

Fig. 11 shows electrical load and PV production profiles as well as exemplary results of a simulation run for a first model of the PtGtX system of the H-BRS hydrogen lab. Parameters of the electrolyzer (530 W max.,  $\eta_{HG} = 0.38$ ) and fuel cell (temperature-dependent polarization curve with the parameters of Fig. 9(b)) as calibrated above are implemented. Synthetic, but typical PV and load profiles are used. They are part of a collection of simulation scenarios representing a full year for optimizing sizing of components. Here, only time series of the power of the components as well the state-of-charge of the battery and MHS tank are shown.

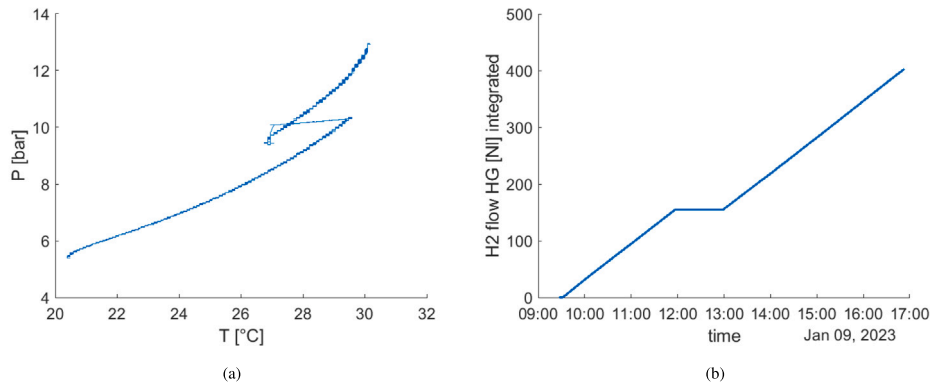


Fig. 7. Exemplary experimental results for hydrogen generation and absorption (for the same working day as in Fig. 5): pressures vs. temperatures (a); aggregated flow values (b).

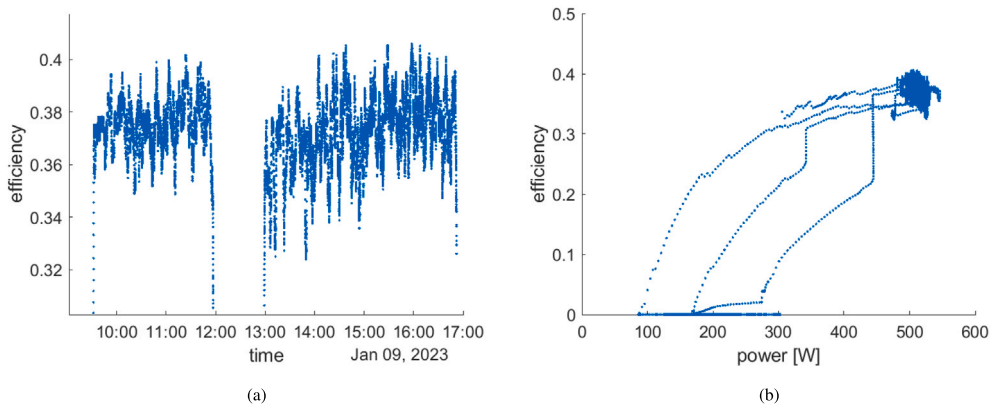


Fig. 8. Experimental results for hydrogen generation and absorption: efficiency  $\eta_{HG}$  vs. time (a) and power (b).

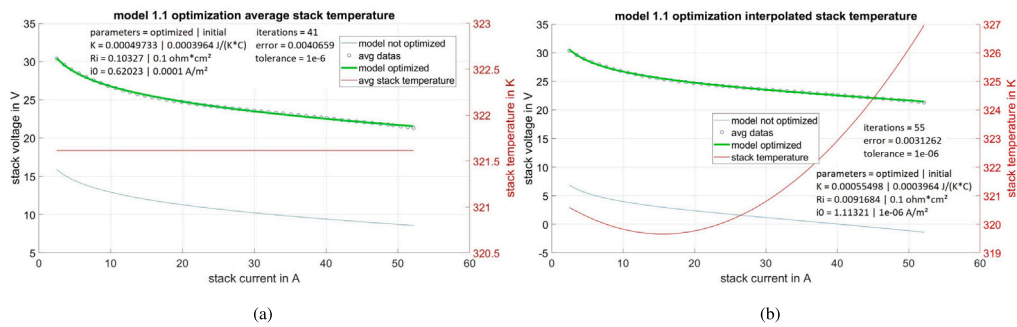


Fig. 9. Results of the parameter calibration: polarization curve of the fuel cell with fixed  $T$  (a) and varying  $T$  (b).

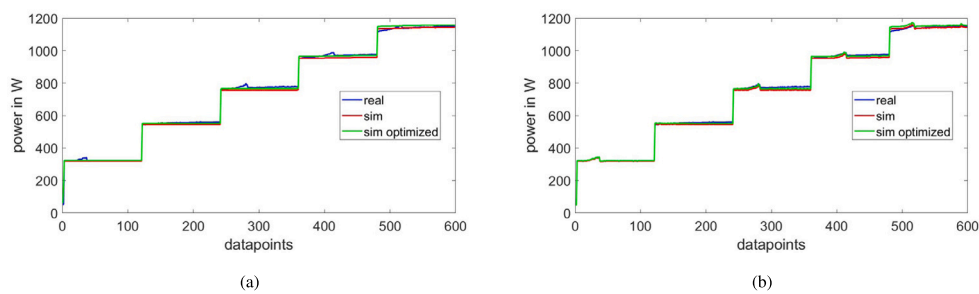


Fig. 10. Results of the parameter calibration for the dynamic behavior of the fuel cell in case of load jumps: the setpoints of an estimated  $I_{stack,est}$  from  $I_{load}$  are used (a), the measured  $I_{stack}$  is used (b).

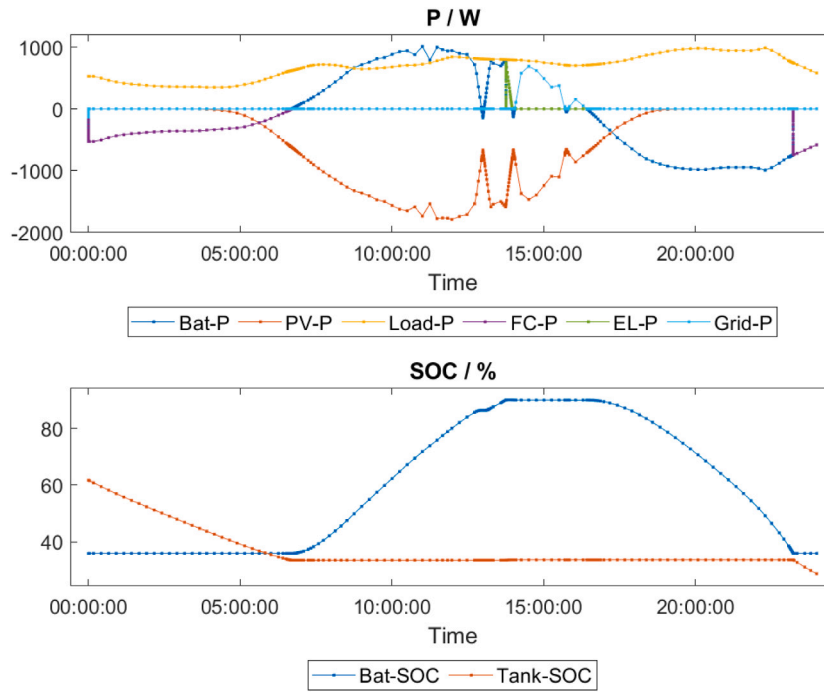


Fig. 11. Results of a simulation run for the H-BRS lab model. Results of battery (Bat-P), fuel cell (FC-P), electrolyzer (EL-P), public grid (Grid-P), PV and load power (on top) as well as the state-of-charge (SOC) values of the buffer battery and the MHS (at the bottom) are shown.

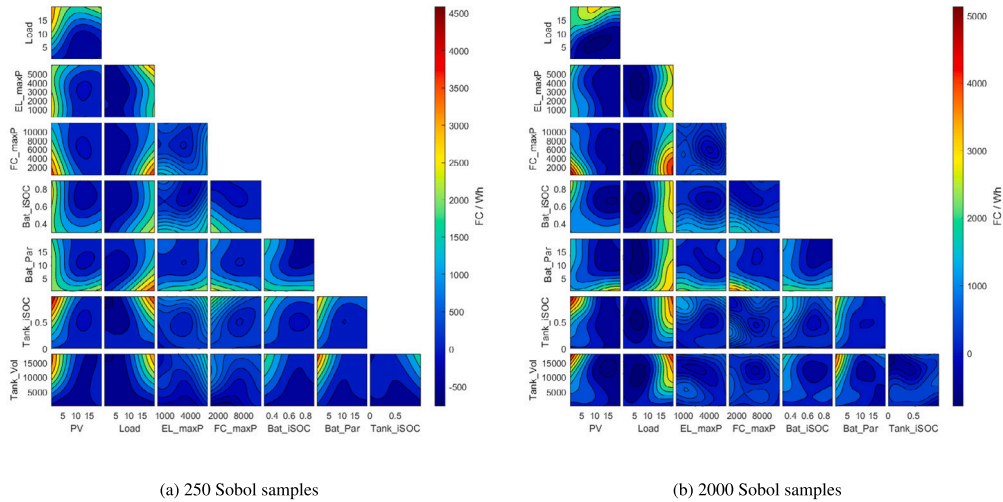


Fig. 12. Comparison of 250 (a) and 2000 (b) Sobol sample RBF metamodel output slices for fuel cell energy balance.

The design of the control algorithm is crucial for an efficient HESS, but is beyond the scope of this study and deserves future work. The rudimentary control algorithm implemented here works by prioritizing the battery first, MHS second and grid last in order to direct power to or from, depending on the difference of generated and consumed power. Due to the sizing and range of each component, in most simulation cases the battery is smaller than the MHS. In combination with the prioritization of the battery, this aids the role distribution of short-term and long-term storage. As can be seen from the power and SOC time series, even the rudimentary control algorithm used here supports this.

### 3.4. Metamodel of the hydrogen lab model

In order to create the RBF metamodel, a DoE is used to run simulations for 2000 Sobol samples. While 2000 simulations would take about 16.6 h for an average time of 30 s per simulation, the computation

time is drastically reduced to 2.1 h with parallel computing on 8 cores (AMD Ryzen 7 3700X). Table 2 shows the required time to create a metamodel, to compute  $4^8 = 65\,536$  output values and the accuracy of those values for the 8 input parameters. The accuracy is computed by comparing the metamodel output values against simulation results of a  $4^8$  full factorial DoE, taking the median of the absolute deviation ( $MAD_{median}$ ) of all values for one output, for example the energy balance of the fuel cell. The  $MAD_{median}$  of all outputs, i.e. electrolyzer, fuel cell, battery, MHS and grid is used to compute a mean ( $MMAD_{median}$ ) that indicates the accuracy of the metamodel.

Fig. 12 visualizes the output of the metamodel for the energy produced by the fuel cell (in 24 h) depending on the value of the input parameters. The 8-dimensional parameter space is shown in slices of all combinations of two input parameters each and their influence on the output. For every slice, the other 6 input parameters are set to 50%

**Table 2**

Statistics on computational time for creating RBF metamodels, computing 65 536 values and their accuracy for different sample numbers, and optimization of  $\sigma$  in RBF multiquadric with total optimization time, iterations per optimization, time per iteration for different sample numbers, with initial value of  $\sigma = 0.05$ . Computed on an Intel Core i5-1135G7.

Samples	Comp. time for		$MMAD_{median}$	$t_{optim}$	$n_{iter}$	$\frac{t_{optim}}{n_{iter}}$	opt. $\sigma$
	Creation	4 <sup>s</sup> evals					
250	3 ms	0.6 s	4.9%	42 s	38	1.1 s	0.47
500	11 ms	0.9 s	4.2%	52 s	38	1.3 s	0.47
1000	46 ms	1.5 s	3.6%	68 s	36	1.9 s	0.38
1500	115 ms	2.5 s	3.4%	97 s	36	2.7 s	0.34
2000	220 ms	4.2 s	3.3%	161 s	34	4.7 s	0.32

of the interval in which they are varied with the DoE. The outputs of the 250 and 2000 samples metamodel are similar, but still show differences, which can be seen especially well for regions of high or low power.

When creating and using the metamodel consisting of  $N$  samples, an  $N \times N$  matrix is created for the RBF. This means that the time required for computations increases by the square. In Table 2 can be seen that although the time required to create an RBF metamodel follows the quadratic trend, for the case of up to 2000 samples the time is negligible ( $\leq 220$  ms). The computation time for 65 536 metamodel output value calculations increases with the number of used samples (42 s for 250 samples, 161 s for 2000 samples), however the quadratic trend is also quite small on these scales. For the optimization of the parameter  $\sigma$  (multiquadric kernel of RBF), Table 2 shows that depending on the number of samples a different optimal  $\sigma$  is found. The time required for the optimization increases with the number of samples, while the time for every iteration of the optimization agrees with the evaluation time. The metamodells with more samples presumably require less iterations, because the found optimum is closer to the initial value of  $\sigma$ .

In Fig. 12 the 250-sample metamodel output slices look “smoothed” compared to the 2000-sample slices, which is certainly the effect of using less samples. Considering the results in Table 2, the accuracy is comparable and sufficient for the intended use case of finding regions of interest with efficient global optimization (EGO methods) and improving local approximations by running new simulations. To be more specific, the 250-sample metamodel speeds up evaluation of the simulation model by a factor of more than 262.1 at 4.9% accuracy, the 2000-sample one by a factor of more than 32.7 at 3.3% accuracy. Note that the computing time for constructing the simulation samples is included and the by far dominant part since optimization of  $\sigma$  and the 65 536 model evaluations performed sum up to less than 170 s, 65 536 simulation runs on 8 cores to 68 h.

#### 4. Conclusion

The focus of the present paper is on a real HESS system at the H-BRS using a PEM electrolyzer, PEM fuel cell, metal hydride storage and buffer battery. Parameter identification is discussed for the combined electrolyzer and MHS subsystem, and for the fuel cell a novel multistage parameter calibration process based on a multi-dimensional Newton method is introduced. An analysis of the experimental results of the electrolyzer reveals strong pressure–temperature dependencies and also a certain effect on the efficiency of the cell. The temperature increase of the MHS is significant and cannot be neglected for optimal energy management. It is highly dependent on the starting pressure and temperature of the MHS, the electrolyzer and the environment. Calibrating the fuel cell stack parameters with 10 A-jump experiments, the step-up part of the accumulated consumed power requires an average correction of 1.31%, the step-down part 3.65%.

A new multiphysical energy system simulation tool, MEgy, has been introduced to address the lack of fast, deeply linked multiphysical

modeling in existing simulators that include electrical and fluid transport, and electrochemical subnets together with their thermodynamics. MEgy can resolve, in particular, electrolyzer plants and fuel cell plants in more detail compared to MYNTS and can itself provide characteristic maps or profiles for a usage in MYNTS and similar simulators. A first, rudimentary control strategy is implemented which fulfills a main goal in most simulation cases of HESS systems for the battery to act as short-term and the MHS as long-term storage. A successful MEgy simulation model of the PtGtX HESS at H-BRS is established.

In order to find the optimal sizing of the components for given scenarios, metamodel-based simulation optimization is used. The simulations required for classical optimization iterations are replaced by significantly faster evaluations of an RBF metamodel constructed from simulation results, enabling considerably faster optimization over one year. Five metamodells are constructed for the PtGtX HESS considered here: The smallest one speeds up evaluation of the simulation model by a factor of more than 262.1 at 4.9% accuracy, the largest by a factor of more than 32.7 at 3.3% accuracy.

The main focus of future work is to improve energy and thermal management of components in HESS systems. A mathematical model of the electrolyzer shall be developed to keep temperature effects and waste heat as small as possible. Such a thermal management shall then be integrated into optimizing sizing and performance of HESS systems further. The results of the optimization process for parameters of the fuel cell show that the model can accurately approximate hydrogen consumption scenarios under temperature changes and large load jumps, paving the way for further energy management development. In order to increase accuracy further, a model for approximating time steps and influences of the fuel cell purging shall be implemented based on related technical specifications in [39]. While the mathematical optimization process constructs parameter sets which accurately reproduce measurement data, the actual parameter values cannot be interpreted physically yet. This is a typical, yet seldom discussed open issue in literature. A first way to arrive at physically meaningful values is discussed in [21] for PEM electrolyzers and shall be adapted to fuel cells in future work.

The metamodel shall be used for sizing and control optimization of the HESS in future work, as the accuracy is sufficient for purposes such as performing an efficient global parameter optimization. Local improvement of the optimization can be performed by setting up local metamodells and iterating this process if necessary. To be more specific, the metamodel-based optimization workflow shall form a basis for MHS storage planning, continuing the work conducted in [41], as well as for comparing retrofitted combined heat and power plants with fuel cell plants in [42].

In order to increase performance of simulation even further, MEgy is currently being implemented in the JULIA programming language in addition to the MATLAB version. The recent [43], supervised by the authors, shows that the first Julia package developed is 3.75 times faster than the Matlab version for the district heating networks tested there.

#### CRediT authorship contribution statement

**Michael Bareev-Rudy:** Writing – original draft, Visualization, Validation, Software, Methodology, Formal analysis, Data curation. **Simon Meiswinkel:** Methodology, Data curation. **Malte Pfennig:** Software, Methodology. **Steffen Schedler:** Methodology. **Barbara Schiffer:** Software, Methodology. **Gerd Steinebach:** Writing – original draft, Supervision, Software, Methodology. **Tanja Clees:** Writing – original draft, Supervision, Resources, Methodology, Investigation, Formal analysis, Data curation.

## Declaration of competing interest

The authors declare that they have no known competing financial interests or personal relationships that could have appeared to influence the work reported in this paper.

## Data availability

Data will be made available on request.

## Acknowledgments

This work was supported by the German Federal Ministry for Education and Research [Hydrogen Flagship Project TransHyDE\_FP1 MechaMod, grant number 03HY201N; FHprofUnt FlexHyX project, grant number 13FH172PX8] and the German Federal Ministry for Economic Affairs and Climate Action [MarrakEsH project, grant number 03EN5035F]. The authors would like to thank the anonymous reviewers for their valuable suggestions.

## Appendix A. Supplementary data

Supplementary material related to this article can be found online at <https://doi.org/10.1016/j.enconman.2024.118694>.

## References

- [1] Dawood F, Anda M, Shafiullah GM. Hydrogen production for energy: An overview. *Int J Hydrog Energy* 2020;45(7):3847–69. <http://dx.doi.org/10.1016/j.ijhydene.2019.12.059>.
- [2] Yue M, Lambert H, Pahon E, Roche R, Jemei S, Hissel D. Hydrogen energy systems: A critical review of technologies, applications, trends and challenges. *Renew Sustain Energy Rev* 2021;146:111180. <http://dx.doi.org/10.1016/j.rser.2021.111180>.
- [3] Zhou L, Zhou Y. Study on thermo-electric-hydrogen conversion mechanisms and synergistic operation on hydrogen fuel cell and electrochemical battery in energy flexible buildings. *Energy Convers Manage* 2023;277:116610. <http://dx.doi.org/10.1016/j.enconman.2022.116610>.
- [4] Han G, Kwon Y, Kim JB, Lee S, Bae J, Cho E, Lee BJ, Cho S, Park J. Development of a high-energy-density portable/mobile hydrogen energy storage system incorporating an electrolyzer, a metal hydride and a fuel cell. *Appl Energy* 2020;259:114175. <http://dx.doi.org/10.1016/j.apenergy.2019.114175>.
- [5] Arsad AZ, Hannan MA, Al-Shetwi AQ, Mansur M, Muttaqi KM, Dong ZY, Blaabjerg F. Hydrogen energy storage integrated hybrid renewable energy systems: A review analysis for future research directions. *Int J Hydrog Energy* 2022;47(39):17285–312. <http://dx.doi.org/10.1016/j.ijhydene.2022.03.208>.
- [6] Kavadias KA, Apostolou D, Kaldellis JK. Modelling and optimisation of a hydrogen-based energy storage system in an autonomous electrical network. *Appl Energy* 2018;227:574–86. <http://dx.doi.org/10.1016/j.apenergy.2017.08.050>.
- [7] The MathWorks I. Matlab Simscape fuel cell stack. 2023. URL <https://de.mathworks.com/help/sps/powersys/ref/fuelcellstack.html>.
- [8] Held T. Modellbildung, Simulation und Optimierung einer wasserstoffbetriebenen Autofahre unter Berücksichtigung von Alterungseffekten (Masterthesis), Sankt Augustin, Germany: Hochschule Bonn-Rhein-Sieg, University of Applied Sciences; 2022.
- [9] Stotz G. Szenarientwicklung, Modellbildung und Simulation gekoppelter Energienetze mit lokalen Wasserstoffspeichern (Masterthesis), Sankt Augustin, Germany: Hochschule Bonn-Rhein-Sieg, University of Applied Sciences; 2022.
- [10] Schole J. Modellbildung und Simulation gekoppelter Strom-, Gas- und Wärmenetze mit MATLAB/Simscape und Analyse von Szenarien (Masterthesis), Sankt Augustin, Germany: Hochschule Bonn-Rhein-Sieg, University of Applied Sciences; 2022.
- [11] Heckel, et al. Investigation of dynamic interactions in integrated energy systems. Tech. Rep., Technische Universität Hamburg; 2022. <http://dx.doi.org/10.15480/882.4678>.
- [12] Lohmeier D, Cronbach D, Drauz SR, Braun M, Kneiske TM. Pandapipes: An open-source piping grid calculation package for multi-energy grid simulations. *Sustainability* 2020;12(23). <http://dx.doi.org/10.3390/su12239899>.
- [13] Clees T, Baldin A, Klaassen B, Nikitina L, Nikitin I, Spelten P. Efficient method for simulation of long-distance gas transport networks with large amounts of hydrogen injection. *Energy Convers Manage* 2021;234:113984. <http://dx.doi.org/10.1016/j.enconman.2021.113984>.
- [14] Kunz O WW. The GERG-2008 wide-range equation of state for natural gases and other mixtures: An expansion of GERG-2004. *J Chem Eng Data* 2012;57:3032–91. <http://dx.doi.org/10.1021/jc300655b>.
- [15] Wagner W, Pruss A. The IAPWS Formulation 1995 for the thermodynamic properties of ordinary water substance for general and scientific use. *J Phys Chem Ref Data* 2002;31:387–535. <http://www.iapws.org/relguide/IAPWS-95.html>.
- [16] Clees T, Hornung N, Alvarez ÉL, Nikitin I, Nikitina L, Torgovitskaia I. Cooling circuit simulation I: Modeling. In: Griebel M, Schüller A, Schweitzer MA, editors. Scientific computing and algorithms in industrial simulations: Projects and products of Fraunhofer SCAI. Cham: Springer International Publishing; 2017, p. 61–79. [http://dx.doi.org/10.1007/978-3-319-62458-7\\_4](http://dx.doi.org/10.1007/978-3-319-62458-7_4).
- [17] Steinebach G, Dreistadt DM. Water and hydrogen flow in networks: Modelling and numerical solution by ROW methods. In: Rosenbrock—wanner-type methods. Springer International Publishing; 2021, p. 19–47. [http://dx.doi.org/10.1007/978-3-030-76810-2\\_2](http://dx.doi.org/10.1007/978-3-030-76810-2_2).
- [18] Petrucci A, Barone G, Buonomano A, Athienitis A. Modelling of a multi-stage energy management control routine for energy demand forecasting, flexibility, and optimization of smart communities using a Recurrent Neural Network. *Energy Convers Manage* 2022;268:115995. <http://dx.doi.org/10.1016/j.enconman.2022.115995>.
- [19] Dreistadt DM, Puszkiel J, Bellosta von Colbe JM, Capurso G, Steinebach G, Meilinger S, Le T-T, Covarrubias Guarneros M, Klassen T, Jepsen J. A novel emergency gas-to-power system based on an efficient and long-lasting solid-state hydride storage system: Modeling and experimental validation. *Energies* 2022;15(3). <http://dx.doi.org/10.3390/en15030844>.
- [20] Kushnir R, Ullmann A, Dayan A. Thermodynamic models for the temperature and pressure variations within adiabatic caverns of compressed air energy storage plants. *J Energy Resour Technol* 2012;134(2). <http://dx.doi.org/10.1115/1.4005659>.
- [21] Pfennig M, Schiffer B, Clees T. Thermodynamical and electrochemical model of a PEM electrolyzer plant in the megawatt range with a literature analysis of the fitting parameters. *Int J Hydrog Energy* 2024. <http://dx.doi.org/10.1016/j.ijhydene.2024.04.335>.
- [22] Sharifi Asl S, Rowshanzamir S, Eikani M. Modelling and simulation of the steady-state and dynamic behaviour of a PEM fuel cell. *Energy* 2010;35(4):1633–46. <http://dx.doi.org/10.1016/j.energy.2009.12.010>, Demand Response Resources: the US and International Experience.
- [23] Rossetti I. Modelling of fuel cells and related energy conversion systems. *ChemEngineering* 2022;6(3). <http://dx.doi.org/10.3390/chemengineering6030032>.
- [24] Mann RF, Amphlett JC, Hooper MA, Jensen HM, Peppley BA, Roberge PR. Development and application of a generalised steady-state electrochemical model for a PEM fuel cell. *J Power Sources* 2000;86(1):173–80. [http://dx.doi.org/10.1016/S0378-7753\(99\)00484-X](http://dx.doi.org/10.1016/S0378-7753(99)00484-X).
- [25] Ansari SA, Khalid M, Kamal K, Abdul Hussain Ratlamwala T, Hussain G, Alkahtani M. Modeling and simulation of a proton exchange membrane fuel cell alongside a waste heat recovery system based on the organic rankine cycle in MATLAB/SIMULINK environment. *Sustainability* 2021;13(3). <http://dx.doi.org/10.3390/su13031218>.
- [26] Tang Y, Yuan W, Pan M, Li Z, Chen G, Li Y. Experimental investigation of dynamic performance and transient responses of a kW-class PEM fuel cell stack under various load changes. *Appl Energy* 2010;87(4):1410–7. <http://dx.doi.org/10.1016/j.apenergy.2009.08.047>.
- [27] Steinebach G. From river Rhine alarm model to water supply network simulation by the method of lines. In: Mathematics in industry. Springer International Publishing; 2016, p. 783–92. [http://dx.doi.org/10.1007/978-3-319-23413-7\\_109](http://dx.doi.org/10.1007/978-3-319-23413-7_109).
- [28] Steinebach G. Construction of Rosenbrock–Wanner method Rodas5P and numerical benchmarks within the Julia Differential Equations package. *BIT* 2023;63(2). <http://dx.doi.org/10.1007/s10543-023-00967-x>.
- [29] Costa M, Di Blasio G, Prati M, Costagliola M, Cirillo D, La Villetta M, Caputo C, Martoriello G. Multi-objective optimization of a syngas powered reciprocating engine equipping a combined heat and power unit. *Appl Energy* 2020;275:115418. <http://dx.doi.org/10.1016/j.apenergy.2020.115418>.
- [30] Alirahmi SM, Assareh E, Arabkoohsar A, Yu H, Hosseini SM, Wang X. Development and multi-criteria optimization of a solar thermal power plant integrated with PEM electrolyzer and thermoelectric generator. *Int J Hydrog Energy* 2022;47(57):23919–34. <http://dx.doi.org/10.1016/j.ijhydene.2022.05.196>.
- [31] Wang J, Xue K, Guo Y, Ma J, Zhou X, Liu M, Yan J. Multi-objective capacity programming and operation optimization of an integrated energy system considering hydrogen energy storage for collective energy communities. *Energy Convers Manage* 2022;268:116057. <http://dx.doi.org/10.1016/j.enconman.2022.116057>.
- [32] Soares do Amaral JV, Montevecchi JAB, Miranda RdC, Junior WtdS. Metamodel-based simulation optimization: A systematic literature review. *Simul Model Pract Theory* 2022;114:102403. <http://dx.doi.org/10.1016/j.simpact.2021.102403>.
- [33] Bareev-Rudy M, Steinebach G, Clees T. Optimal sizing and control of a hydrogen-based hybrid energy storage system by means of metamodeling. In: Proc. 22th ECMI conf. on industrial and applied mathematics 2023, jun 26–30, Wrocław, Poland. submitted. 2023.
- [34] Mischner J, Fasold H-G, Heymer J. gas2energy.net - Systemplanerische Grundlagen der Gasversorgung. DIV Deutscher Industrie-Verlag GmbH; 2015, p. 906.

- [35] Mohammadshahi S, Gray E, Webb C. A review of mathematical modelling of metal-hydride systems for hydrogen storage applications. *Int J Hydrog Energy* 2016;41(5):3470–84. <http://dx.doi.org/10.1016/j.ijhydene.2015.12.079>.
- [36] Bedrunka M, Bornemann N, Steinebach G, Reith D. A metal hydride system for a forklift: Feasibility study on on-board chemical storage of hydrogen using numerical simulation. *Int J Hydrog Energy* 2022;47(24):12240–50. <http://dx.doi.org/10.1016/j.ijhydene.2021.05.179>.
- [37] Pei P, Chang Q, Tang T. A quick evaluating method for automotive fuel cell lifetime. *Int J Hydrog Energy* 2008;33(14):3829–36. <http://dx.doi.org/10.1016/j.ijhydene.2008.04.048>, TMS07: Symposium on Materials in Clean Power Systems.
- [38] Heliocentris Academia International GmbH. New Energy Lab V1.5, Experiment Guide, System at Hochschule Bonn-Rhein-Sieg in operation since 2022. URL [https://www.heliocentrisacademia.com/product/new\\_energy\\_lab](https://www.heliocentrisacademia.com/product/new_energy_lab).
- [39] Ballard Power Systems Inc. MAN5100319 - FCgen 1020ACS product manual - rev. 0A. 2011, Public information available at the URL. URL [https://www.ballard.com/about-ballard/publication\\_library/product-specification-sheets/fcgen1020-spec-sheet](https://www.ballard.com/about-ballard/publication_library/product-specification-sheets/fcgen1020-spec-sheet).
- [40] Heliocentris Academia International GmbH. Metal Hydride Storage Canister MHS 800. URL [https://www.heliocentrisacademia.com/product/metal\\_hydride\\_storage\\_canisters](https://www.heliocentrisacademia.com/product/metal_hydride_storage_canisters).
- [41] Schedler S, Meilinger S, Clees T. Data analysis and parametrization of a regional housing sector for hydrogen storage planning. In: *Procs. 18th conf. sustainable development of energy, water and environment systems (SDEWES) 2023*, sep 24-29, Dubrovnik, Croatia. 2023.
- [42] Schiffer B, Pfennig M, Clees T. Comparison of hydrogen-based power plant technologies with a focus on district heating in Germany. In: *Procs. 18th conf. sustainable development of energy, water and environment systems (SDEWES) 2023*, sep 24-29, Dubrovnik, Croatia. 2023.
- [43] Rieck F. Implementierung eines JULIA-packages zur Simulation gekoppelter Strom-, Gas- und Wärmenetzwerke (Masterthesis), Sankt Augustin, Germany: Hochschule Bonn-Rhein-Sieg, University of Applied Sciences; 2023.